

## 0.1 Introduction

The physics program of an EIC imposes several challenges on the design of a detector, and more globally the extended interaction region, as it spans a wide range in center-of-mass energy, different combinations of both beam energy and particle species, and several different physics processes. The various physics processes encompass inclusive measurements ( $ep/A \rightarrow e' + X$ ), which require detection of the scattered lepton and/or the full scattered hadronic debris with high precision; semi-inclusive processes ( $ep/A \rightarrow e' + h + X$ ), which require detection in coincidence with the scattered lepton of at least one (current or target region) hadron; and exclusive processes ( $ep/A \rightarrow e' + N'/A' + \gamma/m$ ), which require detection of all particles in the reaction. The figures in section 0.2 demonstrate the differences in particle kinematics of some representative examples of these reaction types, as well as differing beam energy combinations. For these plots the directions of the beams are defined as for HERA at DESY: the hadron beam is in the positive  $z$  direction ( $0^\circ$ ) and the lepton beam is in the negative  $z$ -direction ( $180^\circ$ ).

## 0.2 Kinematic Coverage

### 0.2.1 $y$ Coverage

Figure 1 shows the  $x - Q^2$  plane for two different center-of-mass energies. In general, the correlation between  $x$  and  $Q^2$  for a collider environment is weaker than for fixed target experiments. However, an important consideration are the extreme values of the inelasticity  $y$ . At large  $y$  radiative corrections become large as can be seen in figure 7.25 of the INT report. There are at least two ways to address this: One is to calculate radiative corrections, and two is to detect all particles and reconstruct the electron. This was successfully done at HERA using the Jacquet-Blondel method [?, ?]. As shown in figure 1 cuts placed in the range between  $y=0.8-0.9$  seem reasonable. At very low  $y$ , radiative corrections are small. However, at fixed center of mass energy,  $s$ , the systematic uncertainty in measurements of  $y$  directly propagates into uncertainties in  $x$  (note:  $Q^2 = sxy$ ) which can be large and are independent of particle detection. By taking data at different values of  $s$  one may circumvent the problem of making measurements at extreme values of  $y$ , for instance, at lower  $s$  one can study kinematics at higher values of  $y$ , as can be seen from comparing the two panels of Figure 1. This may become relevant for some semi-inclusive and exclusive processes. The advantages and disadvantages of this solution are discussed in the two machine-specific detector sections of this chapter. The coverage of each setting is given by the product of  $y \times s$ . With a low  $y_{min}$  cut one thus needs fewer settings in  $s$ . However, this is an important consideration for L/T separations, for instance, for measurements of  $F_L$  where one needs to have full  $y$ -coverage at all energies.

### 0.2.2 Angle and momentum distributions

Figure 2 shows the momentum versus scattering angle distributions in the laboratory frame for pions originating from semi-inclusive reactions, for different lepton and proton beam energy combinations. For lower lepton energies pions are scattered more in the forward (ion) direction. With increasing lepton beam energy, the hadrons increasingly populate the central region of the detector, and at the highest lepton energies hadrons are even largely produced going backward (i.e. in the lepton beam direction). The kinematic distributions

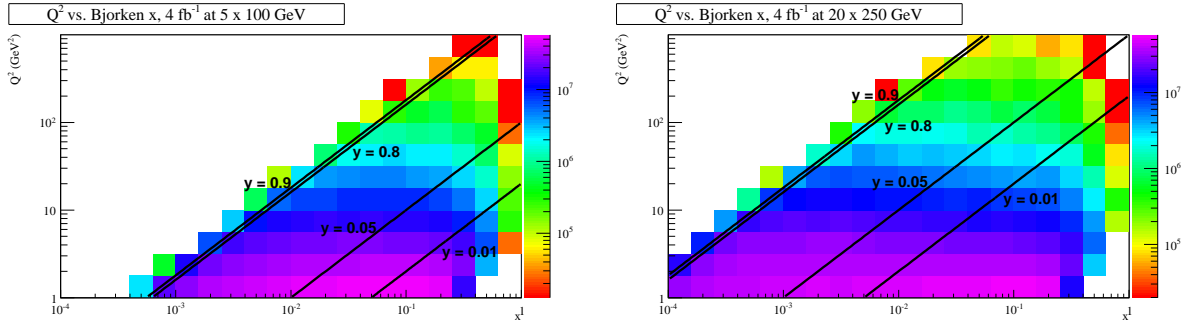


Figure 1: The  $x - Q^2$  plane for center-of-mass energy 45 GeV (left) and 140 GeV (right). The black lines indicate different  $y$ -cuts placed on the scattered lepton kinematics.

for kaons and additional protons/anti-protons, applying the same cuts as for pions, are essentially identical to those of the pions. The distributions for semi-inclusive events in electron nucleus collisions may be slightly altered due to nuclear modification effects, but the global features will remain.

Fig. 2 also indicates a shift of the momentum range of pions towards higher momenta in the central-angle region for higher lepton energy, to typical momenta of about 10 GeV/c, which has implications for the required particle identification (PID). For the higher hadron momenta, typically in the forward ion direction and also in the backward direction for higher lepton beam energies, the most viable detector technology is a Ring-Imaging Cherenkov (RICH) detector with dual-radiators. In the central detector region a combination of high resolution time-of-flight (ToF) detectors (preferentially with timing resolutions  $\delta t \sim 10$ ps), a DIRC or a proximity focusing Aerogel RICH may be adequate detector technologies.

For certain kinematics the hadrons (both charged and neutral) will be produced in the backward ion direction, and need to be disentangled from the scattered leptons. The kinematic region in rapidity  $\eta$  over which hadrons and photons need to be suppressed with respect to electrons shifts to more negative rapidity with increasing center-of-mass energy. This can be cross-correlated with the angular and momentum patterns for scattered leptons. For the lower center-of-mass combination, electron, photon and charged hadron rates are roughly comparable at 1 GeV/c total momentum and  $\eta = -3$ . For the higher center-of-mass energy, electron rates are a factor of 10-100 smaller than photon and charged hadron rates, and comparable again at a 10 GeV/c total momentum.

This adds another requirement to the detector: good electron identification. The kinematic region in rapidity  $\eta$  over which hadrons and also photons need to be suppressed, typically by a factor of 10 - 100, shifts to more negative rapidity with increasing center-of-mass energy.

Measuring the ratio of the lepton energy and momentum,  $E'_e/p'_e$ , typically gives a reduction factor of  $\sim 100$  for hadrons. This requires the availability of both tracking detectors (to determine momentum) and electromagnetic calorimetry (to determine energy) over the same rapidity coverage. This availability also immediately suppresses the misidentification of photons in the lepton sample, by requiring that a track must point to the electromagnetic cluster. The availability of good tracking detectors over similar coverage as electromagnetic calorimetry similarly aids in  $y$  resolution at low  $y$  from a lepton method only (see earlier), as the angular as well as the momentum resolution for trackers are much better than for

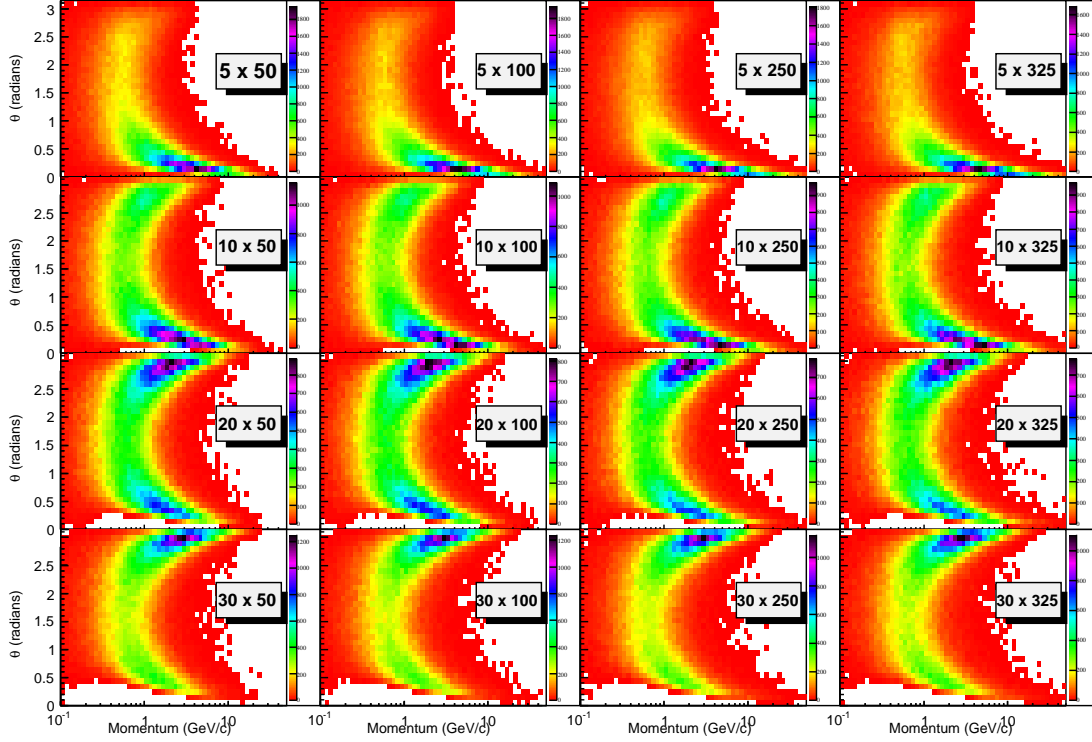


Figure 2: Momentum vs. scattering angle in the laboratory frames for pions from non-exclusive reactions. The following cuts have been applied:  $Q^2 > 1 \text{ GeV}^2$ ,  $0.01 < y < 0.95$  and  $0.1 < z < 0.9$

electromagnetic calorimeters. The hadron suppression can be further improved by adding a Cherenkov detector to the electromagnetic calorimetry. Combining the electromagnetic calorimeter response and the response of Cherenkov detectors may especially help in the region of low-momentum scattered leptons, about 1 GeV/c. Other detector technologies, such as transition radiation detectors, may provide another factor 100 hadron suppression for lepton momenta greater than 4 GeV/c.

There is specific interest in extracting structure functions with heavy quarks from semi-inclusive reactions for mesons with charm or bottom. To measure such structure functions,  $F_2^c$ ,  $F_L^c$ , and  $F_2^B$ , it is sufficient to tag the charm and the bottom quark content via detection of additional leptons (electron, positron, muons) to the scattered lepton. The leptons from charmed mesons can be identified via a displaced vertex of the second lepton ( $\tau > \sim 150 \mu\text{m}$ ). This can be achieved by integrating a high-resolution vertex detector into the detector design. For measurements of the charmed (bottom) fragmentation functions, or to study medium modifications of heavy quarks in the nuclear environment, at least one of the charmed (bottom) mesons must be completely reconstructed to have access to the kinematics of the parton. This requires, in addition to measuring the displaced vertex, good particle identification to reconstruct the meson via its hadronic decay products, e.g.  $D_0 \rightarrow K^\pm + \pi^\mp$ .

Figure 3 shows the momentum versus scattering angle distributions for hadrons following from exclusive reactions, in the laboratory frame and for different beam energy combinations. The general patterns are as in Fig. 2. However, for imaging studies through

exclusive reactions involving light mesons, a  $Q^2$  cut must be applied for a valid partonic interpretation. Since exclusive low- $Q^2$  hadrons are produced in the forward direction, a  $Q^2 > 10 \text{ GeV}^2$  cut drastically changes the kinematic patterns from figure 2. The upper panels of figure 3 shows how the momentum distribution of exclusive pseudoscalar mesons changes with lepton and proton energy.

The most challenging constraints on the detector design for exclusive reactions compared to semi-inclusive reactions is, however, not given by the scattered hadron, but from the detection of the exclusive final state.

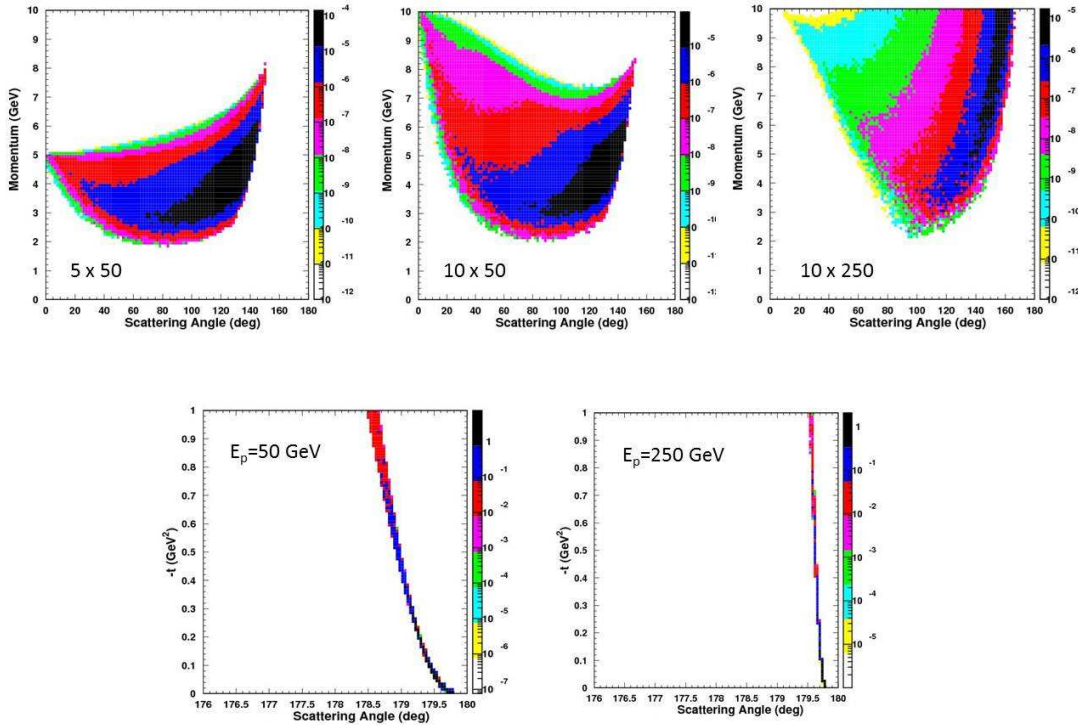


Figure 3: The momentum distribution of the exclusive hadronic final state as a function of the scattering angle for three different center of mass energies,  $\sqrt{s}=31.6, 44.7, 100 \text{ GeV}$  (upper three panels), and the  $t$  distribution as a function of scattering angle of the recoiling baryon in exclusive reactions for proton beam energies  $E_p=50 \text{ GeV}$  and  $250 \text{ GeV}$  (lower two panels). A cut of  $Q^2 > 10 \text{ GeV}^2$  is applied to select the kinematic range of interest for exclusive processes. For lower center of mass energies, the momentum distribution tends towards more central scattering angles and covers lower momenta. The angle of the recoiling hadronic system is directly and inversely correlated with the proton energy. It thus decreases with increasing proton energy. For instance, as shown here, the baryon scattering angle ranges to about  $1\text{-}2^\circ$  at a proton energy of  $50 \text{ GeV}$  and is reduced to one fifth of that as the proton energy increases to  $250 \text{ GeV}$ .

### 0.2.3 Recoil Baryon angles and $t$ resolution

For exclusive reactions it is extremely important to ensure the remaining nucleon (or the nucleus) remains intact during the scattering process. Hence, one has to ensure exclusivity

by measuring all products. In general, for exclusive reactions, one wishes to map the four-momentum transfer (or Mandelstam variable)  $t$  to the hadronic system, and then obtain an image by a Fourier transform, for  $t$  from zero up to about 1-2 GeV.

The bottom panels of figure 3 show one of the most challenging constraints on the detector and interaction region design from exclusive reactions - the need to detect the full hadronic final state. The figures show the correlation between  $t$  and proton energy, and illustrate that the remaining baryonic state goes very much in the forward ion direction, but far less so for lower proton energies, which are thus much easier to peel off from any beam-stay-clear area. Furthermore,  also shows the benefits of lower proton energies for imaging in terms of the  $t$ -resolution?

Even at a proton energy of 50 GeV, the proton scattering angles only range to about  $1-2^\circ$ . At proton energies of 250 GeV, this number is reduced to one/fifth. In all cases, one obtains small to extremely small scattering angles, extending to or completely within the  $0.5^\circ$  angular detector cutoff often used above. Because of this, the detection of these protons, or more general recoil baryons, is extremely dependent on the exact interaction region design and will therefore be discussed in more detail in the machine-dependent part of this chapter.

### 0.3 Detector and Interaction Region Layout

#### 0.3.1 Detector Design for eRHIC

Combining all the requirements described in section 0.2 and in the physics chapters before, a schematic view of the emerging dedicated eRHIC detector is shown in fig. 4.

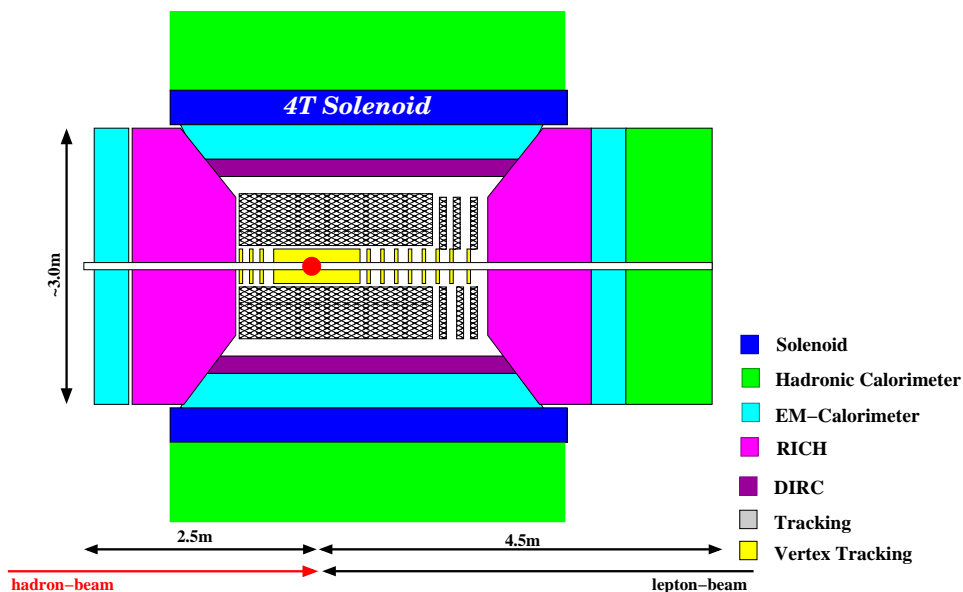


Figure 4: A schematic view of a dedicated EIC detector. Details of the GEANT-3 model can be found at [https://wiki.bnl.gov/eic/index.php/Detector\\_Design](https://wiki.bnl.gov/eic/index.php/Detector_Design).

It is important to have equal rapidity coverage for tracking and electromagnetic calorimetry. This will provide good electron identification and give better momentum and angular

resolutions at low inelasticity  $y$  than with an electro-magnetic calorimeter alone.

The significant progress in the last decade in the development of Monolithic Active Pixel Sensors (MAPS), in which the active detector, analog signal shaping, and digital conversion take place in a single silicon chip (i.e. on a single substrate; see [?] and references therein), provides a unique opportunity for a  $\mu$ -vertex detector for an eRHIC detector. As a result, CMOS pixel detectors can be built with high segmentation, limited primarily by the space required for additional shaping and digital conversion elements. The key advantage of CMOS MAPS detectors is the reduced material required for the detector and the (on substrate) on-detector electronics. Such detectors have been fabricated and extensively tested (see e.g. [?]) with thicknesses of about 50  $\mu\text{m}$ , corresponding to 0.05% of a radiation length.

For tracking at larger radii there are several possibilities, which need to be investigated first through Monte Carlo studies for position resolution and material budget, and later through R&D and building prototypes. The two most prominent options for the barrel tracker are a TPC and a cylindrical GEM-Tracker. For large radii forward tracking GEM-Trackers are the most likely option. The projected rates for a luminosity of  $10^{34} \text{ cm}^{-2} \text{ s}^{-1}$  range, depending on the center-of-mass energy, between 300 and 600 kHz, with an average of 6 to 8 charged tracks per event. These numbers do not impose strong constraints on the technology for a tracker.

Due to the momentum range to be covered the only solution for PID in the forward direction is a dual radiator RICH, combining either Aerogel with a gas radiator like  $\text{C}_4\text{F}_{10}$  or  $\text{C}_4\text{F}_8\text{O}$  if  $\text{C}_4\text{F}_{10}$  is no longer available, or combining the gas radiator with a liquid radiator like  $\text{C}_6\text{F}_{14}$ .

In the barrel part of the detector several solutions are possible, as the momenta of the majority of the hadrons to be identified are between 0.5 GeV and 5 GeV. The technologies available in this momentum range are high resolution ToF detectors ( $t \sim 10\text{ps}$ ), a DIRC or a proximity focusing Aerogel RICH.

For the electromagnetic calorimetry in the forward and backward direction a solution based on  $\text{PbWO}_4$  crystals would be optimal. The advantages of such a calorimeter would be a small Molière radius of 2 cm and a factor of two better energy resolution and higher radiation hardness than, for example, lead-glass. To increase the separation of photons and  $\pi^0$ s to high momenta and to improve the matching of charged tracks to the electromagnetic cluster, it would be an advantage to add, in front of all calorimetry, a high resolution preshower. We follow for the barrel part of the detector the concept of very compact electromagnetic calorimetry (CEMCal). A key feature is to have at least one preshower layer with 1–2 radiation lengths of tungsten and silicon strip layers (possibly with two spatial projections) to allow separation of single photons from  $\pi^0$  to up  $p_T \approx 50 \text{ GeV}$ , as well as enhanced electron-identification. A straw-man design could have silicon strips with  $\Delta\eta = 0.0005$  and  $\Delta\phi = 0.1$ . The back section for full electromagnetic energy capture could be, for cost effectiveness and good uniformity, an accordion Lead-Scintillator Design, which would provide gain uniformity and the ability to calibrate the device. A tungsten- and silicon-strip-based preshower would also be a good solution for the forward and backward electromagnetic calorimetry.

To achieve the physics program as described in earlier sections it is extremely important to integrate the detector design into the interaction region design of the collider. Particularly challenging is the detection of forward-going scattered protons from exclusive reactions, as well as of decay neutrons from the breakup of heavy ions in non-diffractive reactions. The eRHIC design features a 10 mrad crossing angle between the protons or heavy ions during

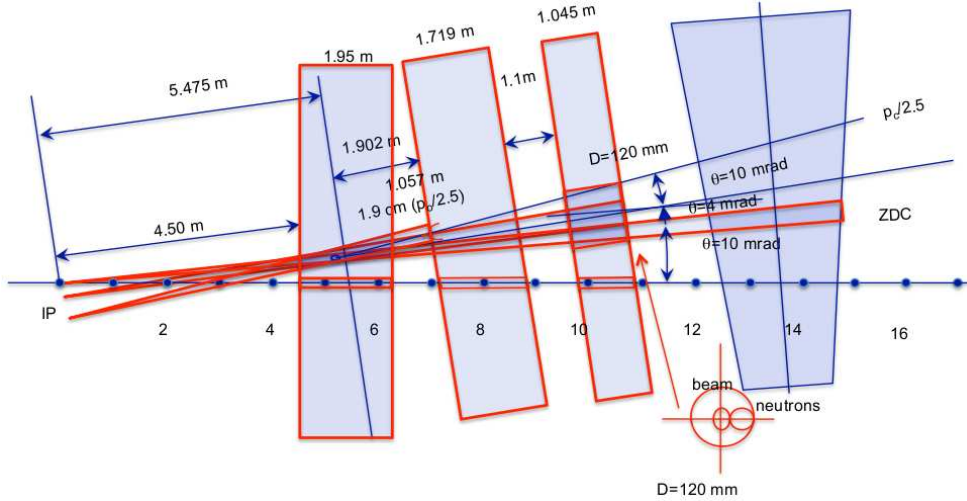


Figure 5: Schematic view of the eRHIC interaction region design in the direction of the outgoing hadron beam.

collisions with electrons. This choice removes potential problems for the detector induced by synchrotron radiation. To obtain luminosities higher than  $10^{34} \text{ cm}^{-2} \text{ s}^{-1}$ , very strong focusing close to the IR is required to have the smallest beam sizes at the interaction point. A small beam size is only possible if the beam emittance is also very small. The focusing triplets are 4.5 meters away from the interaction point (IP). The strong focusing quadrupoles induce very large chromaticities. The current eRHIC design has its highest values of the amplitude betatron functions of the same size as the present operating conditions of the RHIC collider. In addition the design allows a correction of the first, second and third order chromaticities by using sextupoles at the triplets as well as 180 degrees away from the quadrupoles source

While the above accomplishes a small-emittance electron beam, the ions and protons need to be cooled by coherent electron cooling to have small emittance. The eRHIC interaction region design relies on the existence of small emittance beams with a longitudinal RMS of 5 cm, resulting in a  $\beta^* = 5 \text{ cm}$ . Strong focusing is obtained by three high-gradient quadrupole magnets using recent results from the LHC quadrupole magnet upgrade program (reaching gradients of 200 T/m at 120 mm aperture). To ensure the previously described requirements from physics are met, four major requirements need to be fulfilled: high luminosity ( $> 100$  times that of HERA), the ability to detect neutrons, measurement of the scattered proton from exclusive reactions (i.e. DVCS), and the detection of low-momentum protons ( $p \sim p_0/2.5$ ) from heavy-ion breakup. The eRHIC IR design fulfills all these requirements: the first magnet in the high focusing quadrupole triplet is a combined function magnet producing a 4 mrad bending angle of the ion/proton beam. The 120 mm diameter aperture of the last quadrupole magnet allows detection of neutrons with a solid angle of  $\pm 4 \text{ mrad}$ , as well as the scattered proton from exclusive reactions, i.e. DVCS, up to a solid angle of  $\sim 9 \text{ mrad}$ . The electrons are transported to the interaction point through the heavy ion/proton triplets, seeing zero magnetic field.

Figure 5 shows the current eRHIC interaction region design in the direction of the outgoing hadron beam. The other side of the IR is mirror symmetric for the incoming

hadron beam. For the outgoing lepton beam we are currently investigating how to best integrate a low scattering-angle lepton tagger.

### 0.3.2 Detector Design for MEIC/ELIC

A global outline of the fully integrated MEIC detector and interaction region is given in Fig. 6. A detailed description of the central detector, as well as the extended interaction region strategy for achieving a full-acceptance detector can be found in the INT10-03 report. In the subsequent subsections we will focus on the main aspects. To achieve full-acceptance, small-angle detection is required on either side of the central detector. The low- $Q^2$  electron detection is relatively simple to incorporate, while the measuring forward and ultra-forward hadronic or nuclear fragments along the ion direction is more challenging. Here, we make critical use of various ingredients of the MEIC detector/interaction region design: i) the 50 mrad crossing angle; ii) the range of proton energies; iii) a small 1-2 Tm dipole field before the ion final focusing magnets to allow high-resolution tracking down to  $0.5^\circ$ ; iv) ion final focusing magnets (FFQs) with apertures sufficient for particles with angles up to at least  $0.5^\circ$ ; and v) a large 20 Tm, large acceptance dipole magnet a few m downstream of the FFQs to peel off spectator particles and allow for very small-angle detection with high resolution (essentially only limited by the intrinsic momentum spread of the beam).

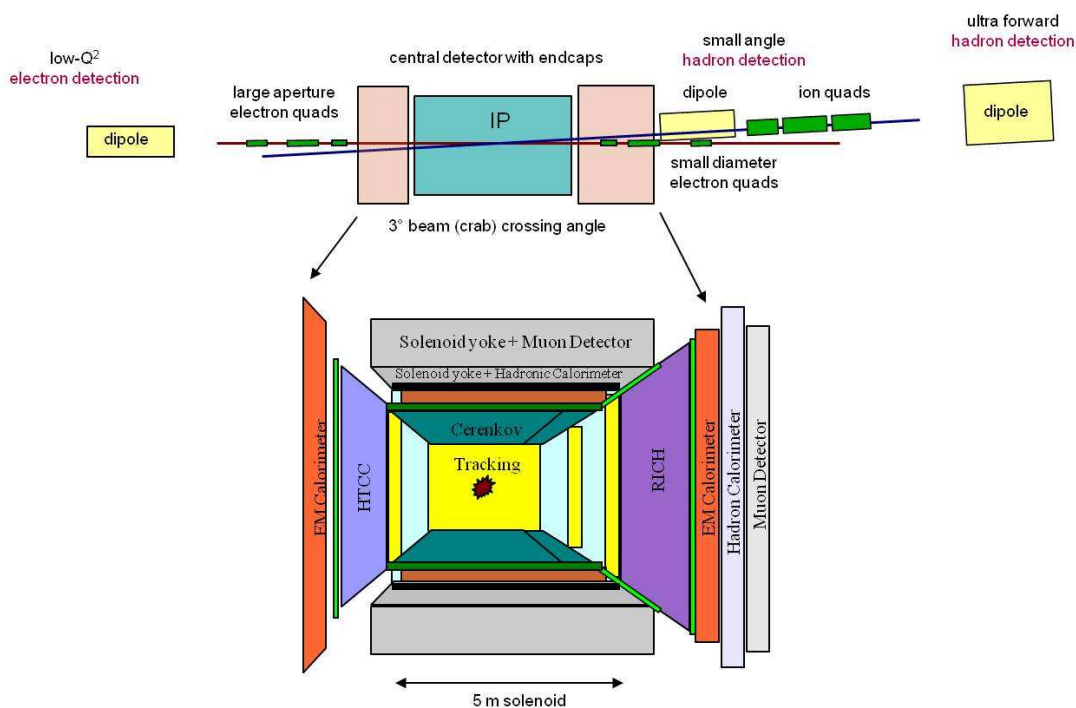


Figure 6: Interaction region and central detector layout, and its placement in the general integrated detector and interaction region. The central detector includes endcaps in both the electron and ion direction.

Detectors will be placed between the FFQs and the 20 Tm dipole, as well as in an extended, magnet-free drift space downstream of it. The apertures of the FFQs provide full neutron acceptance up to  $0.5^\circ$ . The neutrons (and boosted nuclear photons) will be detected in a zero-degree calorimeter (ZDC) on the outside of the ring. In this

configuration, any desired angular resolution can be achieved simply by adjusting the size and distance of the ZDC. This then results in an essentially 100% full acceptance detector.

To minimize synchrotron radiation and improve the small-angle hadron acceptance and resolution, the electron beam travels along the center of the central solenoid, while the proton/ion beam traverses it at the crab crossing angle.

To fulfill the requirement of hermeticity, the central detector will be build around a solenoid magnet (with a length of about 5 m). Due to the asymmetric beam energies, the interaction point (IP) will be slightly offset towards the electron side (2 m + 3 m). This will allow more distance for the tracking of high-momentum hadrons produced at small angles, and a larger bore angle for efficient detection of the scattered beam leptons.

The central detector would contain a three-layer tracker, particle identification, and calorimetry. Particle identification in the central detector would be provided by TOF, and a radially compact detector providing  $e/\pi$ ,  $\pi/K$ , and  $K/p$  identification. The current baseline design includes a DIRC supplemented by a Low-Threshold Cerenkov Counter (LTCC) with  $C_4F_{10}$  or  $C_4F_8O$  gas. The latter would provide  $e/\pi$  separation between 1 and 3 GeV/c, and extend the  $\pi/K$  separation from 4 to 9 GeV/c, but would require 60-70 cm of radial space. Optimizations and alternatives to this baseline design are discussed in more detail in the INT report.

Small-angle tracking in the central detector could be an extension of the vertex tracker, using semiconductor detectors, while larger angles could be covered by planar micropattern detectors (GEMs). On the electron side, where the particle momenta are generally lower, one could also consider drift chambers with a small cell size, in particular for a final tracking region that could be added outside of the solenoid itself. Lepton identification in the endcap will be performed using an electromagnetic calorimeter and a High-Threshold Cerenkov Counter (HTCC) with  $CF_4$  gas or equivalent. The details of hadron identification in the electron endcap can be found in the INT report.

The ion side endcap would have to deal with hadrons with a wide range of momenta, some approaching that of the ion beam. While the small-angle tracking resolution on this side is greatly enhanced by the substantial crossing angle (particles scattered at zero degrees are not moving parallel to the B-field) and dipole in front of the FFQs, the forward tracking would nevertheless greatly benefit from good position resolution (also in front of and after the dipole), making this a priority. To identify particles of various species over the full momentum range, one would ideally want to use a RICH with several radiators, such as aerogel,  $C_4F_{10}$ , and  $CF_4$ . Possible implementation are detailed in the INT report.

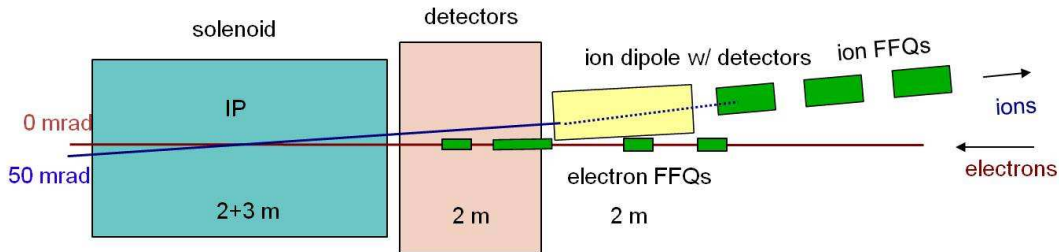


Figure 7: Forward ion detection with 50 mrad crossing angle for the full-acceptance detector. Note that the distance to the final focusing quadrupoles are located 7 m from the IP.

On the ion side, the detection will be performed in three stages, as illustrated in Figure 7.

The first stage is the endcap, which will cover all angles down to the acceptance of the forward spectrometer (several degrees around the ion beam line). This in turn has two stages, one upstream of the ion Final Focus Quadrupoles (FFQs), and one downstream of them. As shown by GEANT4 tracking studies, the acceptance of all stages is matched so that there are essentially no gaps in the coverage. The last stage will cover angles up to at least  $\pm 0.5^\circ$ , even with very relaxed magnet requirements (and hence smaller apertures giving peak fields of no more than 6 T), but with the magnet parameters assumed for the BNL IP, this could be doubled.

The intermediate stage will use a 2 Tm dipole to augment the solenoid at small angles where the tracking resolution otherwise would be poor. The magnet will be about 1 m long and its aperture will cover the distance to the electron beam (corresponding to the horizontal crossing angle of 50 mrad), while the acceptance in the other three directions is not restricted and can be larger. An important feature of the magnet design is to ensure that the electron beam line stays field free. The dipole will have trackers at the entrance and exit, followed by a calorimeter covering the ring-shaped area in front of the first ion FFQ. The intermediate stage is essential for providing a wide coverage in  $-t$ , and to investigate target fragmentation.

The last stage provides the ultra-forward detection that is crucial for detecting recoil baryons and tagging of spectator protons in deuterium as well as other nuclear fragments. The design is heavily integrated with the accelerator, and the 3.5 m long, 20 Tm downstream dipole serves not only as a spectrometer, but also “corrects” the 50 mrad crossing angle, and allows the neutrons to escape on a tangent to the ring, separating cleanly from the beam area before detection. This makes the electron and ions beam lines parallel in the  $\sim 15$  m long drift space after the dipole, with separation of more than 1 m, providing ample space for detectors. With only relatively weak focusing for the small-angle detection (and a beam-stay-clear of  $10\sigma$ ), even the preliminary optics give full angular acceptance for charged particles with momenta of up to 99.5% of the beam momentum (or more than 1.05% of its momentum), and full momentum acceptance for particles scattered at more than about 2 mrad with respect to the central beam. On the other hand, the dipole aperture will be sufficient to accept all off-angle and off-momentum particles that exit the FFQs with the exception of “spectator” protons from deuterium scattered at large angles. These can, however, easily be detected in between the FFQs and the dipole. Tracking studies show that the momentum resolution for particles up to the beam momentum will only be limited by the intrinsic momentum spread of the beam (a few  $\times 10^{-4}$ ), and the angular resolution will also be excellent. This is very important since  $t \sim \theta_p^2 E_p^2$ , and the  $t$ -resolution for instance determines the quality of the 3-D imaging that can be achieved.

### 0.3.3 Bibliography